Study of mechanisms and factors that influence the formation of vortical wake of a heaving airfoil

Z. C. Zheng and Z. Wei

Citation: Physics of Fluids **24**, 103601 (2012); doi: 10.1063/1.4760258
View online: http://dx.doi.org/10.1063/1.4760258
View Table of Contents: http://scitation.aip.org/content/aip/journal/pof2/24/10?ver=pdfcov
Published by the AIP Publishing

Study of mechanisms and factors that influence the formation of vortical wake of a heaving airfoil

Z. C. Zheng and Z. Wei
Department of Aerospace Engineering, University of Kansas, Lawrence, Kansas 66045, USA

(Received 19 April 2012; accepted 17 September 2012; published online 23 October 2012)

A two-dimensional numerical study is performed to investigate the relation between the direction of a deflected wake and the vortex pairing mechanisms. The deflection angle can be correlated with two effective phase velocities defined to represent the trends of symmetry breaking and symmetry holding, respectively. The deflection angle increases with the strength of the vortex pairs, which is associated with the heaving amplitude, frequency, and the free stream Reynolds number. Furthermore, not only the influence of Strouhal number but also those of the two heaving motion components – amplitude and frequency – are studied individually under different Reynolds numbers. The study shows that the deflection angle consistently increases with the difference between the symmetry-breaking phase velocity and symmetry-holding phase velocity. © *2012 American Institute of Physics*. [http://dx.doi.org/10.1063/1.4760258]

I. INTRODUCTION

Flow around oscillating airfoils has received a lot of attention because of its wide variety of applications in the area of micro-aerial vehicles. At the beginning of last century, it was found that flapping airfoils were able to create a normal force to produce both lift and thrust.[1,2] Flapping wings can therefore be used as an alternative of conventional propeller. In the following decades, aerodynamics of flapping airfoils was studied systematically for heaving and pitching motions. Garrick[3] and Theodorsen[4] analytically proved that plunging airfoils generate thrust over a wide frequency range, while pitching only airfoils do so only for high frequencies. Koochesfahani,[5] Jones *et al.*,[6] Lua *et al.*,[7] and Bratt[8] explored the vortex patterns of flapping airfoils both experimentally and numerically.

An interesting phenomenon, a deflected vortex wake, was observed in the flow downstream of a heaving symmetric airfoil by Jones *et al.*[6] Although the heaving motion was symmetric and periodic, the wake deflected to one side of the airfoil rather than locating symmetrically along the line of the mean plunging location of the airfoil. Deflected wakes were also recorded earlier by Bratt[8] in experiments of flow over a symmetrically pitching NACA0015 airfoil. Unsurprisingly, similar deflected wakes were found in flow with asymmetric sinusoidal airfoil motions.[9] However, unlike the cases with asymmetric airfoil motions, this phenomenon, with a pure symmetric sinusoidal heaving motion, only occurred at high Strouhal number that Lai and Platzer[10] defined as $2\pi f^* h^*/U_\infty$, where f^* and h^* are the dimensional frequency and amplitude of the heaving motion, respectively. It was noted[6] that the direction of deflection did not change in numerical simulation, whereas in experiment, small disturbances might influence the flow and randomly change the direction of the deflected wake. Heathcote and Gursul[11] presented that the switching of direction of the deflected wake was quasi-periodic in experiments.

Recently, a number of studies have concentrated on the deflected wake. Lewin and Haj-Hariri[12] showed that the direction of the deflected wake could even be altered in the middle of simulation. Blondeaux *et al.*[13] found a chaotic flow pattern when the heaving amplitude was large, which might be another way to explain the observation in Ref. 12. Zhang *et al.*[14] studied the effect of the geometric shape on the trend of the deflected wake and found that slender foils are easier and faster to form an asymmetric downstream wake. In addition, Lua *et al.*[7] experimentally showed the

interactions between leading edge vortex and trailing edge vortex might lead to a deflected wake. For quantifying the deflection angle, the location of the maximum streamwise velocity in the wake was used to determine the deflection angle.[11,15,16] Godoy-Diana *et al.*[17] proposed a vortex dipole model to provide a quantitative prediction of the symmetry breaking wake based on two consecutive counter-rotating vortices in the wake. A symmetry-breaking criterion based on the phase velocity and idealized self-advection velocity of vortex dipole was discussed. More recently, Liang *et al.*[18] found that the wake of a heaving airfoil with a larger Reynolds number would form a larger deflection angle.

In the present study, deflected wakes of a symmetric heaving airfoil with a zero angle of attack are investigated numerically in 2D. An improved immersed-boundary method[19] (IBM) is used for the numerical simulation. The numerical method is validated with a heaving airfoil case in Ref. 12 first. Then factors that influence the wake deflection, including deflection direction and vortex pairing mechanisms, Strouhal number, frequency, amplitude, and Reynolds number, are investigated in detail. Following the vortex pairing concept introduced in Ref. 17 and the definition of deflection angle in Ref. 15, the deflection angle can be correlated with the symmetry-breaking and symmetry-holding effective phase velocities.

II. NUMERICAL METHOD

The immersed-boundary method is an effective way to simulate flow around a moving structure. A direct-forcing IBM[19] is selected for simulation in this study.

The following governing equations for incompressible fluid flow are used:

$$\frac{\partial \mathbf{u}}{\partial t} + \mathbf{u} \cdot \nabla \mathbf{u} = -\nabla p + \frac{1}{\mathrm{Re}} \nabla^2 \mathbf{u} + \mathbf{F}, \tag{1}$$

$$\nabla \cdot \mathbf{u} = 0, \tag{2}$$

where $\mathbf{F}$ is the body forcing term representing the virtual boundary force. In each time step, the forcing term acts as a velocity compensator in order to minimize the error between the desired (physical) boundary velocity and the computed velocity on the boundary surface. The definition of the forcing term is

$$\mathrm{F} = \mathbf{S} + \nabla p - \frac{1}{\mathrm{Re}} \nabla \mathbf{u} + \frac{1}{\Delta t}(\mathbf{V} - \mathbf{u}), \tag{3}$$

where $\mathbf{V}$ is the velocity vector of the airfoil surface, and Re is the Reynolds number defined as $\rho U_\infty c/\mu$, where U_∞ is the free stream velocity and c the chord length of the airfoil. All the variables are non-dimensionalized with the same characteristic parameters. The boundary force has non-zero values only on the boundary surface, while zero anywhere else

$$\mathbf{F} = \begin{cases} \mathbf{f}_G & \text{for the internal - layer grid points} \\ 0 & \text{elsewhere.} \end{cases} \tag{4}$$

The term $\mathbf{S}$ in Eq. (3) is the convection term expressed as

$$\mathbf{S} = (\mathbf{u} \cdot \nabla)\mathbf{u}. \tag{5}$$

The momentum equation, Eq. (1), is solved on a staggered Cartesian grid by using a 2nd order differencing scheme, in which the diffusion term is discretized with a semi-implicit scheme. The Adams-Bashforth scheme is used for the convection. First-order time-marching is employed. The incompressibility condition, Eq. (2), is satisfied by solving a Poisson equation for pressure with a correction process. The Poisson equation is solved by using MUDPACK. This scheme is able to reach overall 2nd order accuracy. More information and detailed descriptions of this method can be found in Ref. 19.

This scheme has been proved capable of simulating moving objects in the flow field.[19–22] For simulating airfoil heaving problems, the current scheme is further validated by comparing velocity

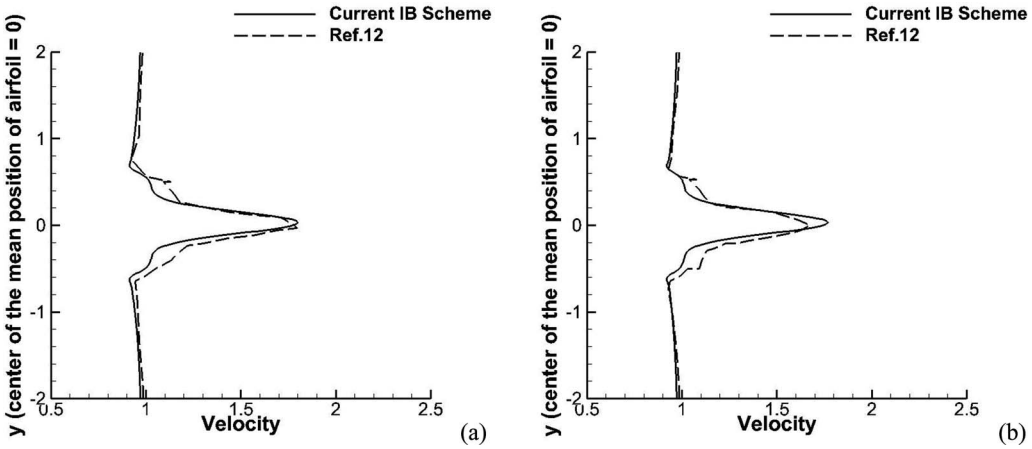

FIG. 1. Comparisons of velocity profiles calculated one chord-length downstream of the trailing edge of the airfoil with the results in Fig. 16 of Ref. 12. (a) Reduced frequency $k = 4.706$; (b) $k = 4.444$.

profiles in Ref. 12. The comparisons in Fig. 1 show a good agreement with the results in Ref. 12 for the analysis of velocity profiles downstream of a heaving airfoil. More specifically, note that there are good matches for the maximum values of the velocity profiles near the center position of the motion. As stated earlier, this location of the maximum velocity in the wake will be used to determine the deflection angle of the asymmetric wake.[11,15,16]

The sinusoidal heaving motion of a symmetric airfoil, a NACA0012 airfoil, is specified as

$$\begin{aligned} y(t) &= h \sin(kt), \\ k &= 2\pi f. \end{aligned} \tag{6}$$

Again, all the equations and variables are dimensionless. The characteristic length and velocity are the airfoil chord length and the free stream velocity, respectively. The frequency, f, and reduced frequency, k, in Eq. (6) are, respectively, $f = f^* c/U_\infty$ and $k = 2\pi f = 2\pi f^* c/U_\infty$. The simulation is performed for a heaving airfoil under four different Reynolds numbers (Re = 200, 300, 400, and 500) and three Strouhal numbers ($V_p = 2\pi f^* h^*/U_\infty = kh = 0.96$, 1.08, and 1.2). The Strouhal number, which is the product of reduced frequency and dimensionless heaving magnitude, is a considered a primary factor that influences the wake of a heaving airfoil.[6,7,9,10,12,15]

The computational domain size selected for this study is 19.2×12.8, shown in Fig. 2. The size of the computational domain is selected so that the size of the domain does not influence the results. The size also fits the appropriate number of grid points for using the FFT-based Poisson solver. The airfoil is located at 7-unit lengths downstream of the inlet flow boundary to leave sufficient space for reducing the effect of the inlet boundary condition. The grid size is $\Delta x = \Delta y = 0.0125$, which provides an acceptable grid-resolution-independent solution for all computational cases in this study after a grid-size convergence study. The Dirichlet-type boundary condition is employed at the inlet for velocity; the symmetry boundary condition is used for both of the upper and lower boundaries; and the outlet is specified with the Neumann-type boundary condition. All velocity profiles presented in this paper were averaged over four airfoil oscillation cycles after the simulation results became periodic.

III. DEFLECTION MECHANISMS AND VORTEX PAIRING

Previous studies reported that the vortex deflection direction is affected by the initial direction of the heaving motion.[6,10,15] This is also confirmed in the current study, as shown in Fig. 3. When the airfoil starts moving upward at the beginning of the heaving motion, the wake deflects downward, and vice versa.

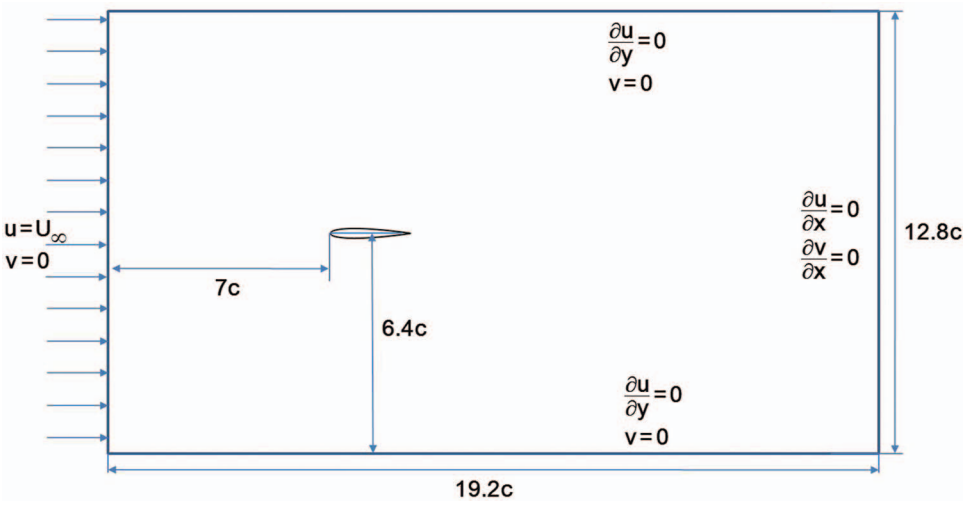

FIG. 2. Definition sketch of set-up of simulations in this study.

This phenomenon is attributed to the pairing pattern of the wake vortices downstream of the airfoil. Figure 3(a) is a case when the airfoil starts periodic heaving with an initially upward motion. Figure 3(a) shows that the distance between vortices "A" and "B" is longer than that between vortices "B" and "C." According to the Biot-Savart vortex induction law, a shorter distance amounts to a stronger vortex interaction. Therefore, vortices "B" and "C" are recognized as a pair instead of "A" and "B," indicating a strong interaction between "B" and "C." Since the negative vortex (darker gray - blue online in Fig. 3) is rotating clockwise and the positive vortex (lighter gray - red online in Fig. 3) counter-clockwise, such a pairing pattern induces a downward motion. This downward

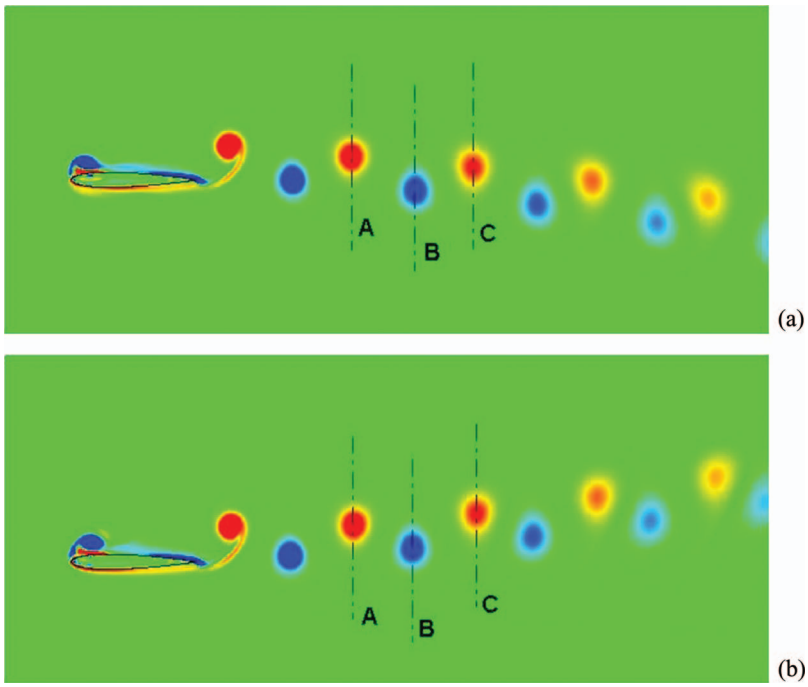

FIG. 3. Vorticity contours for the case of $k = 10$, $h = 0.12$, and $\mathrm{Re} = 400$: (a) the heaving starts with an upward motion; (b) the heaving starts with a downward motion. The dashed lines indicate the approximate center of a vortex. The contour color range is from -30 to 30.

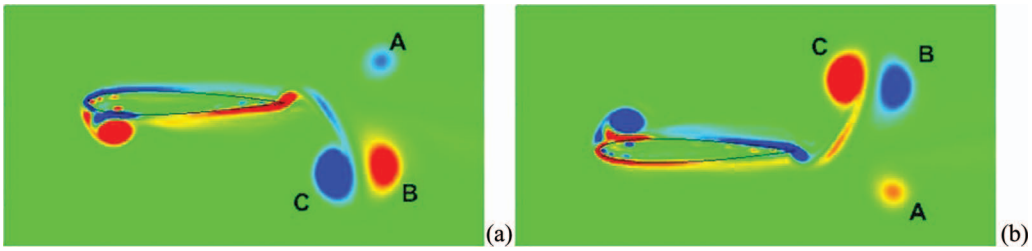

FIG. 4. The pairing competition among the first few vortices of a heaving airfoil, (a) with an initially upward motion; (b) with an initially downward motion.

motion thus results in a downward vortex wake deflection. The situation in Fig. 3(b) is when the airfoil starts with a downward motion. The wake deflection is then in the direction opposite to the case in Fig. 3(a). The vortex pair now formed by "A" and "B" in Fig. 3(b), with a positive vortex on the left and a negative vortex on the right, causes an upward wake vortex deflection.

Following the vortex pairing argument stated above, if the distances between two adjacent vortices are all equal, no deflection should be detected. Several no-deflection cases shown later in the paper will confirm this claim.

Now the follow-up question is why the different vortex pairing patterns occur when the starting motion is upward versus downward. Figure 4 shows the vorticity field at the nascent stages after the airfoil starts to move. It can be seen when the airfoil starts with an upward motion in Fig. 4(a), a starting vortex "A" in the negative sense (clockwise) is generated at the trailing edge. This is because the total lift on the airfoil is negative during the initial upward motion, which is created by an overall circulation around the airfoil in the positive sense. A strong positive sign vortex "B" is generated in the consecutive downward motion, followed by a strong vortex negative sign vortex "C" generated during a later upward motion shown in Fig. 4(a). Due to its lower strength, the starting negative vortex "A" loses the pairing competition with the positive vortex "B" in the wake against the stronger negative vortex "C." Such a pairing, as discussed in the previous paragraph, leads to a downward deflection of the wake. Vice versa, the opposite pairing pattern and thus deflection direction can be seen in Fig. 4(b) when the airfoil starts with a downward motion.

To detect the wake deflection trend quantitatively, Godoy-Diana *et al.*[17] proposed a symmetry-breaking condition depending on the vortex pair (the dipole) structure and the vortex phase speed. We extend this condition by making use of the effective phase velocity to quantitatively define the trends of symmetry breaking and symmetry holding. In the dipole structures (between I and II, and II and III) shown in Fig. 5, the wake tends to deflect downward. The effective phase velocity for a vortex dipole, U_p^*, is then defined as

$$U_p^* = U_{dipole} - (U_{phase} - U_\infty)\cos\alpha. \tag{7}$$

As the deflection is downward in this case, the symmetry-breaking effective phase velocity is calculated based on a dipole that induces the downward motion on the pair of vortices in the dipole. In this case, the symmetry-breaking dipole is represented by vortices II and III, which is the same as the pair selection stated previously. The other pair, vortices I and II, which induces an upward motion in the dipole, is to produce a symmetry-holding effective phase velocity and considered a symmetry-holding dipole. The definition of the variables in Eq. (7) follows those in Ref. 17. Specifically, U_{phase} in Eq. (7) is the averaged x-direction velocity of the motion of the two vortex centers in dipole. The center of a vortex is defined as the location of the local maximum vorticity. And U_{dipole} is calculated as

$$U_{dipole} = \frac{\Gamma}{2\pi\xi} \tag{8}$$

and ξ and α are defined in Fig. 5. For the circulation of the dipole, Γ, it is calculated using the method of vorticity area integration in the rectangular area indicated in Fig. 5. The choice of

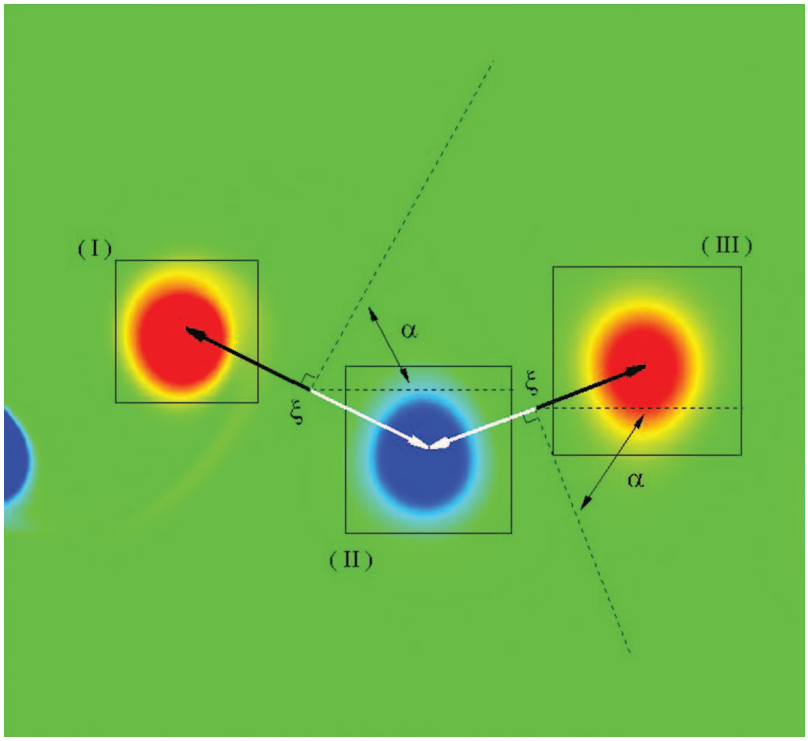

FIG. 5. Parameters used in calculating the effective phase velocities.

rectangular integration contours, instead of the elliptical ones that would have better followed the vortex shape, was made in order to avoid errors from interpolation of the velocity data.[17] The size of the rectangular area is determined by using Gaussian fits, $\exp(-x_i^2/\sigma_i^2)$, along the vertical and horizontal axes centered on positions of the maxima and minima of vorticity. The sizes of the vortex along the x- and y-direction are defined as $2\sigma_i$. The circulation value is the average circulation of the two vortices in the dipole.

We calculated the effective phase velocities of symmetry-breaking and symmetry-holding for the cases shown in Fig. 4. When the wake is deflected either downward (Fig. 4(a)) or upward (Fig. 4(b)), for both cases, the effective symmetry-breaking phase velocity is 0.32, while the effective symmetry-holding phase velocity is 0.21. This is primarily due to the fact that ξ in the symmetry-breaking dipole is smaller than that in the symmetry-holding dipole, which is the same factor to determine vortex pairing as discussed earlier. Since the symmetry-breaking effective velocity is greater than the symmetry-holding effective phase velocity, the wake deflects. Subsequent discussions will make rigorous use of this criterion.

IV. DISCUSSION OF THE FACTORS INFLUENCING WAKE DEFLECTION

A. Effects of the Strouhal number versus the individual effects of the reduced frequency and amplitude

In the discussion of the magnitude of the wake deflection angle, the previous work put more concentration on the effect of the Strouhal number only.[10,15] The current study is the first that has investigated the effect of amplitude and frequency individually on the wake deflection angle. A general consensus in the previous work[7,10,12,15] was that a larger value of V_p is related to a larger deflection angle. However, it was reported[6,7] that in some cases, a flow with larger Strouhal number might not show any wake deflection. Another exception, illustrated in Fig. 6, is that the case with

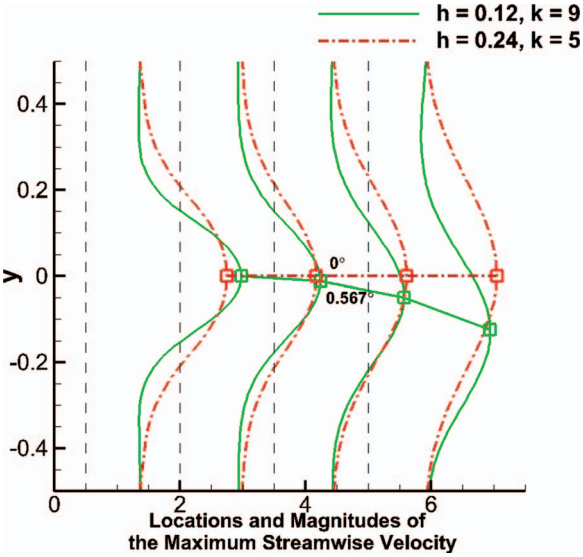

FIG. 6. Streamwise velocity profiles downstream of the airfoil with $h = 0.12$, $k = 9$ (dashed-dotted lines) and $h = 0.24$, $k = 5$ (solid lines). Dashed lines indicate four locations in the flow direction (x-direction) for the downstream distances from the airfoil TE to where the velocity profiles are recorded. Rectangular symbols imply locations of maximum velocity.

$h = 0.12$ and $k = 9$ has a larger deflection angle than the case with $h = 0.24$ and $k = 5$, although the latter has a larger Strouhal number ($V_p = 1.2$) than the former ($V_p = 1.08$).

The way to express the deflection angle in terms of maximum values in velocity profiles in Fig. 6 follows that of Ref. 15. The zero value in the y axis is the mean position of the airfoil heaving motion. Four vertical dashed lines indicate the downstream distances from the trailing edge of the airfoil to where the velocity profiles are recorded. These locations are 0.5, 2, 3.5, and 5 in the x-direction downstream of the trailing edge. The shape of the velocity profiles in Fig. 6 indicates the velocity magnitude at a particular location. Rectangular symbols, which show the locations of maximum value of each profile, are formed to represent the wake deflection angle. Numerical values of deflection angle (i.e., 0° and 0.567° in Fig. 6) are calculated based on the vertical and horizontal location differences of maximum values sampled at the two locations of 0.5 and 2. The type of graphs as in Fig. 6, with omitted curves for velocity profiles, will be frequently employed in the following discussion to compare the wake deflection angles.

Figure 7 shows that the deflection angle increases as V_p increases by increasing the reduced frequency, k, at a fixed heaving amplitude[10,15] ($h = 0.12$ and 0.16, respectively). In this case, the magnitude of maximum downstream velocity also increases, as the symbols on curves with the same line type (solid or dotted-dashed, indicating $h = 0.12$ and 0.16, respectively) from the same location increase their magnitudes in the abscissa direction. The increasing velocity magnitude is in consistence with the fact that higher heaving frequency leads to higher input power from the airfoil, which provides more propulsive force.[9,12]

Figure 7 also confirms the individual effect of reduced frequency and magnitude at a same V_p that is the product of the these two factors. Each of the cases is represented by square, diamond, or circle symbols, and has the same V_p values of 1.2, 1.08, and 0.96, respectively. Note the symbols with solid lines have a lower magnitude and higher frequency than the ones with dashed-dotted lines. The closer distance between the two vortices in a dipole, which appears in the cases of higher frequency such as in Fig. 8(a), gives rise to stronger interactions between the vortices that therefore create a larger angle of deflection in the wake. The cases with higher frequency generate more vortices within the same distance downstream of the airfoil. In Fig. 8, the frequency in the higher frequency case is twice the low frequency case, while the V_p value remains the same as 1.2, the highest V_p value among the cases in Fig. 7. In this particular case, the lower frequency case, with $h = 0.24$ and $k = 5$, even does not have a deflected wake. As stated earlier, the pairing of the vortices into a dipole

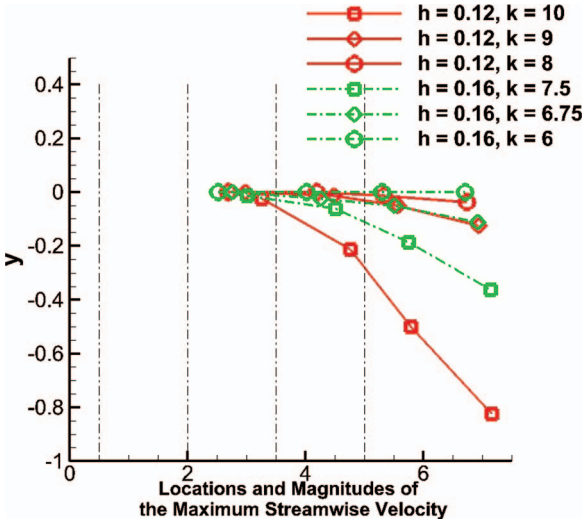

FIG. 7. The vertical location of the maximum value of downstream x-direction velocity profiles for cases with Re = 500, where $y = 0$ is the mean location of the heaving airfoil, and $x = 0$ is the location of the trailing edge of the airfoil.

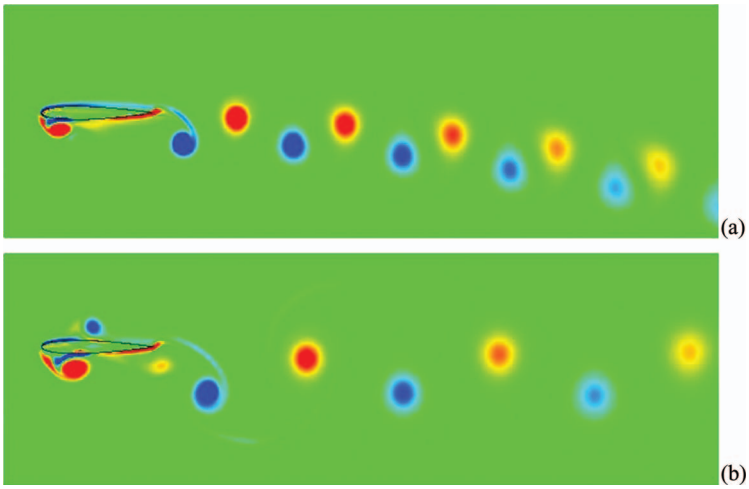

FIG. 8. Vorticity contours of cases with the same $V_p = 1.2$, (a) $h = 0.12$, $k = 10$ and (b) $h = 0.24$, $k = 5$.

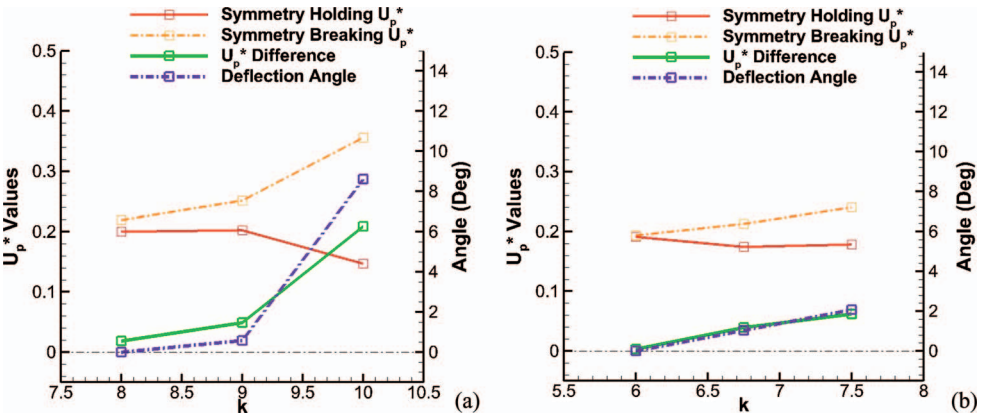

FIG. 9. Deflection angles and effective phase velocities versus the reduced frequency for cases presented in Fig. 7. (a) $h = 0.12$ and (b) $h = 0.16$.

and their interactions are the reason that the wake deflects. Such a pairing pattern does not show in the lower frequency case in Fig. 8(b), where the vortices are evenly distributed like a symmetric, reversed von Karman vortex street.[7,17]

At the same time, by comparing the two wakes in Figs. 8(a) and 8(b), each individual vortex at the same distance downstream the airfoil has almost the same strength in both the higher frequency and lower frequency cases. However, the higher frequency case has twice the number of vortices in the wake with a non-symmetric pairing pattern. This again proves that the vortex pairing pattern is the reason for the wake deflection, not just the vortex strength itself that is somehow related to Strouhal number (when Reynolds number is fixed).

The criterion based on the effective phase velocities presented in Sec. III has been applied in the cases here to check its applicability. Figure 9 contains the plots of the deflection angles and the effective phase velocity versus the reduced frequency for the cases presented in Fig. 7 with $h = 0.12$ and $h = 0.16$, respectively. In both cases in Fig. 9, when the deflection angle increases with the reduced frequency, the symmetry-breaking effective phase velocity apparently increases

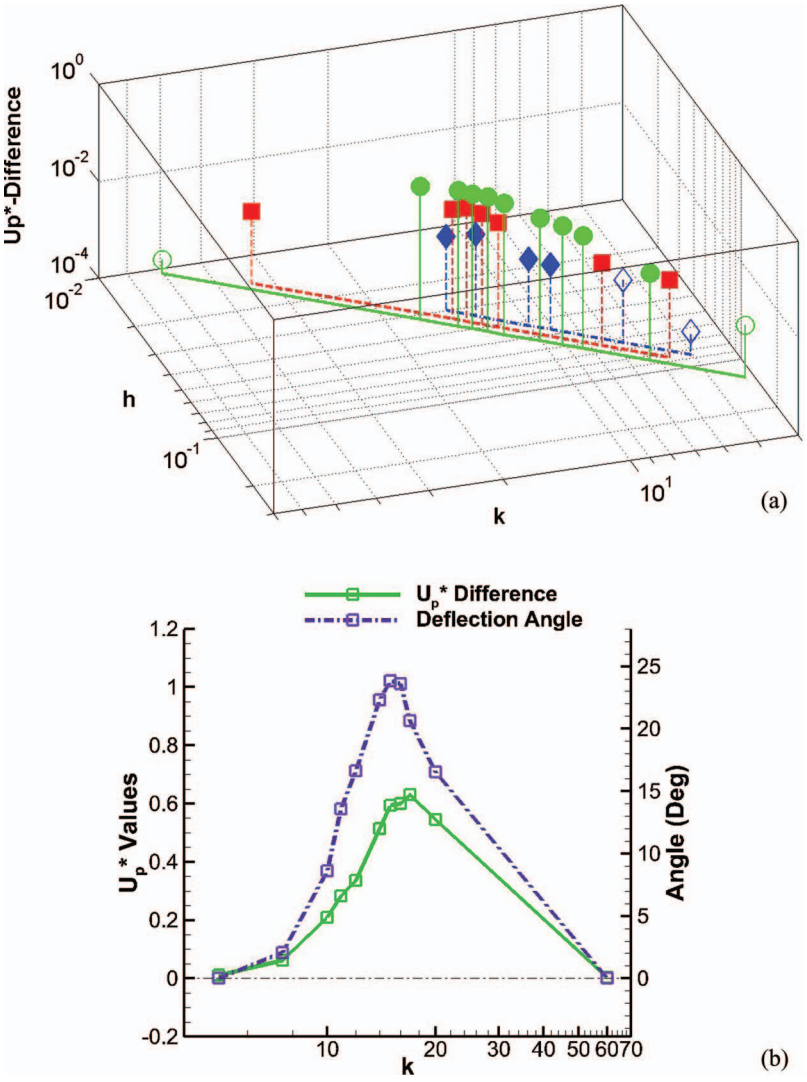

FIG. 10. Deflection angles and the difference between the symmetry-breaking and symmetry-holding effective phase velocities versus the reduced frequency k and heaving amplitude h for the case of Re = 500. (a) Solid lines with circle markers: $V_p = 1.2$; dashed lines with square markers: $V_p = 1.08$; dashed-dotted lines with diamond markers: $V_p = 0.96$. Solid markers: deflected wakes; hallowed markers: symmetry wakes. (b) A particular case of $V_p = 1.2$.

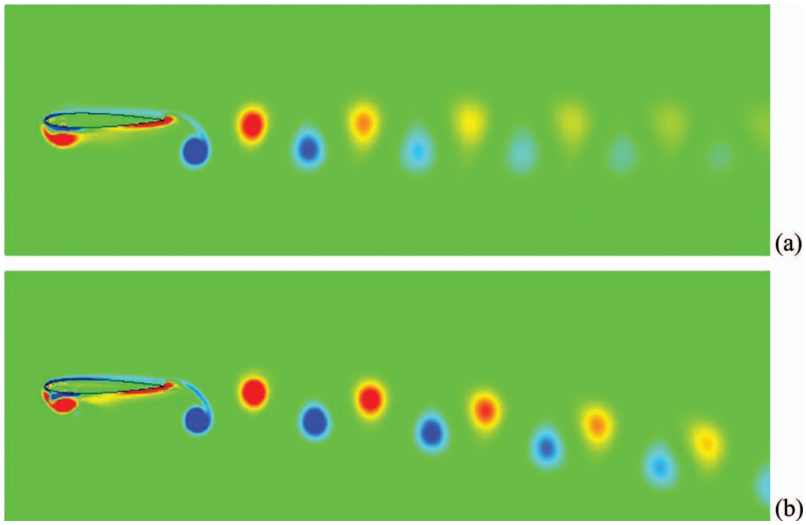

FIG. 11. Vorticity contours at the beginning of the down-stroke for the case of $h = 0.12$, $k = 10$ with Re $= 200$ (a) and Re $= 400$ (b).

while the symmetry-holding phase velocity either decreases slightly or remains almost the same. This result shows when the difference between the two effective phase velocities increases, the deflection angle increases. Such a trend reaffirms the use of effective phase velocity to correlate with the deflection angle.[17]

Figure 10(a) presents the results from a study of the deflection behavior in a wider range of reduced frequencies and heaving amplitude at three Strouhal numbers, $V_p = 0.96$, 1.08, and 1.2. It confirms that the deflection occurs in a regime of moderate heaving amplitude and frequency.[7,12,15,23]

Furthermore, it should be noted some of previous work[7,10,15] showed that, for a certain value of V_p, the wake does not have any deflection for very small or large values of k, while it has quite a significant deflection at moderate values of k. Figure 10(b) illustrates the relationship between the deflection angle and the difference between the symmetry-breaking and symmetry-holding effective phase velocities at a fixed Strouhal number $V_p = 1.2$. The reduced frequency increases in the range of $5 < k < 60$, with a correspondingly decreasing h value. The results in Fig. 10(b) indicate that the

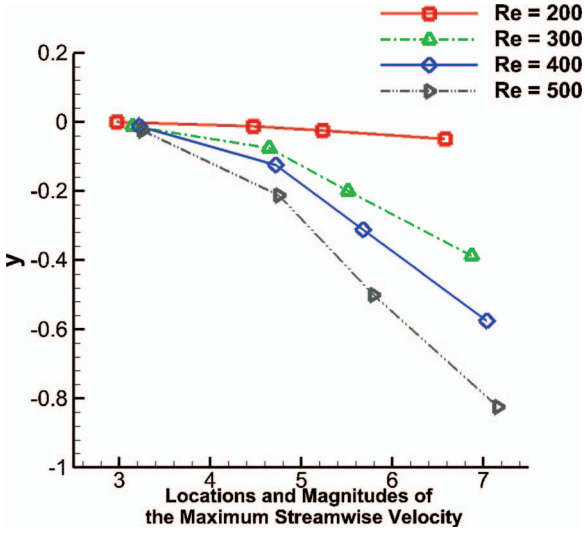

FIG. 12. Deflection angle comparisons with different Reynolds numbers.

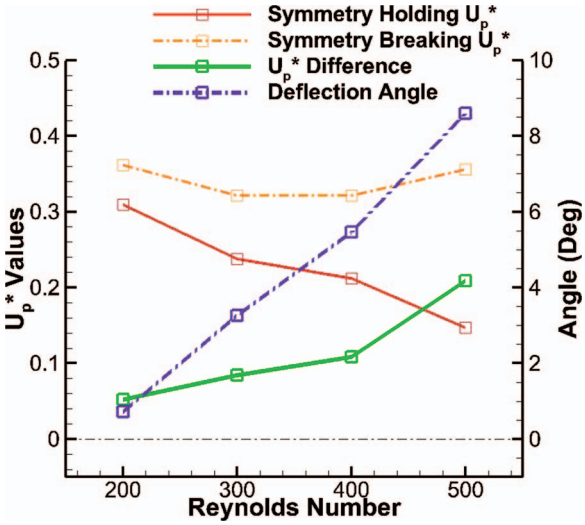

FIG. 13. Deflection angles and effective phase velocities versus the Reynolds number.

deflection angle occurs when the value of k is greater than 7.5. For large values of k, such as 60, with an extremely small h of 0.02 for the same V_p value of 1.2, the flow exhibits a nicely symmetric wake. Therefore, the deflection angle increases to a maximum value at a moderate value of k and reduces towards zero, as the results shown in Fig. 10(b). This trend can also be correlated to the difference between symmetry-breaking and symmetry-holding effective phase velocities. In Fig. 10(b), the deflection angle increases when the difference between the two effective phase velocities increases.

B. Reynolds number effect on the deflection angle

Liang *et al.*[18] claimed that, to their knowledge, they were the first to find the increment of the deflection angle when the Reynolds number increases. The current paper has further studied the mechanism for this phenomenon. The results in Figs. 11 and 12 are for the cases at different Reynolds number but at the same V_p value of 1.2. Figure 11 compares contours of cases with Re = 200 and 400. Apparently, the case with Re = 400 has a larger deflection angle in its wake than the case with Re = 200. The primary factor is the stronger vortices associated with the higher Reynolds number. It is then easily understood that the stronger the vortex pairs, the larger the resultant deflection angles, because the induced motion in the vortex pairs directly causes the deflection. As a higher Reynolds-number flow results in lower vorticity dissipation, Figure 11 illustrates that vortices in the wake of the higher Reynolds number case (Re = 400) decay more slowly than those of the lower Reynolds number case (Re = 200). The vortex pairing pattern also disappears in the lower Reynolds number case, resulting in an almost no-deflecting wake.

The increment of the deflection angle as the Reynolds number increases between 200 and 500 is illustrated in Fig. 12. It also shows that the increase of Reynolds number causes the increase of the magnitude of the maximum velocity, as the symbols indicating the maximum velocity from the same location shift further right in the abscissa direction for larger Reynolds numbers. The correlation between the effective phase velocities and the deflection angle is again presented in Fig. 13. The symmetry-breaking effective phase velocity increases and the symmetry-holding effective phase velocity decreases with the increase of the Reynolds number. This once more correlates the increase of the difference between the two effective phase velocities with the increase of the deflection angle.

V. CONCLUSION

The formation of deflected wakes downstream of a heaving airfoil has been studied numerically. The reason of the deflection is attributed to the vortex pairing pattern in the wake, which causes

a downward deflection wake if the airfoil starts the heaving motion upward, and vice versa. The deflection trend is determined by the competing mechanism between the symmetry-breaking and symmetry-holding effective phase velocities. These velocities are defined and calculated according to the vortex pairing pattern. At the same Strouhal number, the deflection angle achieves its maximum value at moderate reduced heaving frequency. Particularly, at a very small or very large reduced frequency, the pairing pattern that causes the wake deflection disappears, and a symmetric, reversed von Karman street wake is generated. In addition, the Reynolds number also influences the wake deflection. For a fixed Strouhal number, the deflection angle increases with Reynolds number. This is because the vortex strength in the wake is stronger in a high Reynolds number flow, which exacerbates the pairing pattern that causes the wake deflection. In the low Reynolds number cases, the vortices are weaker and the pairing pattern may no longer exist, resulting in a weak, non-deflected wake. Based on this study, it is evident that the size of deflection angle is proportional to the difference between the symmetry-breaking effective phase velocity and the symmetry-holding effective phase velocity. Although this conclusion is based on the results of changing one variable at a time in this study, such as reduced frequency or Reynolds number, the trend should remain the same even under a multi-variable situation.

[1] A. Betz, "Ein Beitrag zur Erklarung des Segelfluges," Z. Flugtech. Motorluftschiffahrt **3**, 269–272 (1912).
[2] R. Knoller, "Die Gesetze des Luftwiderstandes," Flug und Mototecnik (Wien) **3**(21), 1–7 (1909).
[3] I. E. Garrick, "Propulsion of a flapping and oscillating airfoil," NACA Report 567 (1936).
[4] T. Theodorsen, "General theory of aerodynamics instability and the mechanism of flutter," NACA Report 673 (1935).
[5] M. M. Koochesfahani, "Vortical patterns in the wake of an oscillating airfoil," AIAA J. **27**(9), 1200–1205 (1989).
[6] K. D. Jones, C. M. Dohring, and M. F. Platzer, "Experimental and computational investigation of the Knoller-Betz effect," AIAA J. **36**(7), 1240–1246 (1998).
[7] K. B. Lua, T. T. Lim, K. S. Yeo, and G. Y. Oo, "Wake-structure formation of a heaving two-dimensional elliptic airfoil," AIAA J. **45**(7), 1571–1583 (2007).
[8] J. B. Bratt, "Flow patterns in the wake of an oscillating airfoil," Aeronautical Research Council, R&M2773 (1950).
[9] S. Sarkar and K. Venkatraman, "Numerical simulation of incompressible viscous flow past a heaving airfoil," Int. J. Numer. Methods Fluids **51**(1), 1–29 (2006).
[10] J. C. S. Lai and M. F. Platzer, "Jet characteristics of a plunging airfoil," AIAA J. **37**(12), 1529–1537 (1999).
[11] S. Heathcote and I. Gursul, "Jet switching phenomenon for a periodically plunging airfoil," Phys. Fluids **19**(2), 027104 (2007).
[12] G. C. Lewin and H. Haj-Hariri, "Modelling thrust generation of a two-dimensional heaving airfoil in a viscous flow," J. Fluid Mech. **492**, 339–362 (2003).
[13] P. Blondeaux, L. Guglielmini, and M. S. Triantafyllou, "Chaotic flow generated by an oscillating foil," AIAA J. **43**(4), 918–921 (2005).
[14] X. Zhang, S. Ni, S. Wang, and G. He, "Effects of geometric shape on the hydrodynamics of a self-propelled flapping foil," Phys. Fluids **21**(10), 103302 (2009).
[15] K. D. von Ellenrieder and S. Pothos, "PIV measurements of the asymmetric wake of a two dimensional heaving hydrofoil," Exp. Fluids **44**(5), 733–745 (2008).
[16] M. Fuchiwaki, T. Kurinami, and K. Tanaka, "Detailed wake structure behind an elastic airfoil," J. Fluid Sci. Technol. **4**(2), 391–400 (2009).
[17] R. Godoy-Diana, C. Marais, J. L. Aider, and J. E. Wesfreid, "A model for the symmetry breaking of the reverse Benard-von Karman vortex street produced by a flapping foil," J. Fluid Mech. **622**, 23–32 (2009).
[18] C. L. Liang, K. Ou, S. Premasuthan, A. Jameson, and Z. J. Wang, "High-order accurate simulations of unsteady flow past plunging and pitching airfoils," Comput. Fluids **40**(1), 236–248 (2011).
[19] N. Zhang and Z. C. Zheng, "An improved direct-forcing immersed-boundary method for finite difference applications," J. Comput. Phys. **221**, 250–268 (2007).
[20] X. F. Yang and Z. C. Zheng, "Nonlinear spacing and frequency effects of an oscillating cylinder in the wake of a stationary cylinder," Phys. Fluids **22**(4), 043601-1–043601-15 (2010).
[21] N. Zhang and Z. C. Zheng, "Flow/pressure characteristics for flow over two tandem swimming fish," Comput. Fluids **38**(5), 1059–1064 (2009).
[22] Z. Zheng, Z. Wei, and N. Zhang, "Immersed boundary simulations of fast pitching airfoils," in *Proceedings of the 40th AIAA Fluid Dynamics Conference* (Chicago, IL, USA, 2010), AIAA Paper No. 2010-4380.
[23] M. F. Platzer, K. D. Jones, J. Young, and J. C. S. Lai, "Flapping-wing aerodynamics: Progress and challenges," AIAA J. **46**(9), 2136–2149 (2008).